JOURNAL OF AIRCRAFT
Vol. 44, No. 3, May–June 2007

Engineering Notes

ENGINEERING NOTES are short manuscripts describing new developments or important results of a preliminary nature. These Notes should not exceed 2500 words (where a figure or table counts as 200 words). Following informal review by the Editors, they may be published within a few months of the date of receipt. Style requirements are the same as for regular contributions (see inside back cover).

Reduced-Order Aerodynamic Model for Aeroelastic Analysis of Complex Configurations in Incompressible Flow

H. Haddadpour*
Sharif University of Technology, 11365 Tehran, Iran
M. Behbahani-Nejad†
Chamran University of Ahwaz, 61355 Ahwaz, Iran
and
R. D. Firouz-Abadi‡
Sharif University of Technology, 11365 Tehran, Iran

DOI: 10.2514/1.20921

I. Introduction

DETERMINATION of the aeroelastic behavior of subsonic flying vehicles is of great importance. This is partly due to lighter airframe requirements for most applications. Consequently, aeroelastic analyses are becoming regular routines in airframe design processes. Aeroelastic responses can be predicted using aeroelastic codes based on Euler or Navier–Stokes solvers coupled with structural dynamics solvers. However, the major drawback of the aforementioned technique, even for simple three-dimensional geometries, is the required computational time and memory to run the full aeroelastic simulation. In practice, however, simple and accurate methods are needed to predict aeroelastic responses accurately.

The modal analysis technique for structural dynamics analysis is quite routine and widely used for constructing reduced-order models (ROMs). It should be mentioned that this technique was recently applied for unsteady flow analysis, as well. The reduced-order structure and fluid models were employed to construct reduced-order aeroelastic models [1–5] that are mostly applicable to simple geometries such as 2-D airfoils and flat wings in the discrete-time domain.

The objective of this work is to develop a general reduced-order aeroelastic model for 3-D complex geometries in subsonic incompressible flow regimes in the continuous-time domain. In this regard, a boundary element method (BEM) based fluid eigenanalysis solver [6] is integrated with a finite element method (FEM) based modal technique of structural modeling.

Received 6 November 2005; revision received 13 December 2006; accepted for publication 14 December 2006.

*Assistant Professor, Department of Aerospace Engineering, P.O. Box 11365-8639, Azadi Avenue; haddadpour@sharif.edu.
†Assistant Professor, Mechanical Engineering Department.
‡Ph.D. Student, Department of Aerospace Engineering, P.O. Box 11365-8639, Azadi Avenue.

II. Structural Modeling

The modal formulation of structural displacements, along with the Lagrange equations and Galerkin's method, results in a system of equations as follows:

$$\mathbf{M}_s\ddot{\boldsymbol{q}} + \mathbf{C}_s\dot{\boldsymbol{q}} + \mathbf{K}_s\boldsymbol{q} = \boldsymbol{\Xi} \tag{1}$$

where $\boldsymbol{q}$ and $\boldsymbol{\Xi}$ are the vectors of generalized structural coordinates and forces, respectively. Further, the diagonal matrices $\mathbf{M}_s$, $\mathbf{C}_s$, and $\mathbf{K}_s$ are the generalized modal mass, damping, and stiffness matrices, respectively, and are defined as

$$\mathbf{M}_{s_{i,i}} = m_i, \qquad \mathbf{C}_{s_{i,i}} = 2\gamma_i\omega_i m_i, \qquad \mathbf{K}_{s_{i,i}} = m_i\omega_i^2 \tag{2}$$

where m_i, γ_i, and ω_i are the generalized mass, critical damping, and frequency of the ith mode, respectively. Equation (1) is indeed a reduced-order form of the structural dynamics equations and can precisely predict the dynamic behavior of the structure using a few modes.

III. Aerodynamic Modeling

A body with known solid boundaries submerged in a potential flow is considered. The body is assumed to be a closed surface. The governing equation of the outer flow region of the body in the body-fixed frame of reference is

$$\nabla^2\Phi = 0 \tag{3}$$

where Φ is the velocity potential. Assuming that the disturbance of the body motion decays far from the body and applying Green's theorem to Eq. (3), one may obtain the following boundary integral equation at point p on the body surface [6]:

$$2\pi\phi_p = \int_{S_B}\left[\phi\frac{\partial}{\partial\boldsymbol{n}}\left(\frac{1}{r}\right) - \frac{1}{r}\frac{\partial\phi}{\partial\boldsymbol{n}}\right]\mathrm{d}S + \int_{S_w}\Delta\phi_W\frac{\partial}{\partial\boldsymbol{n}}\left(\frac{1}{r}\right)\mathrm{d}S \tag{4}$$

where $\phi = \Phi - \phi_\infty$ is the perturbation potential. Here, S_B and S_W are the integration regions of the body and wake surfaces, respectively. Further, r is the distance from point p to the boundary element $\mathrm{d}S$. The wake is considered to be thin and no aerodynamic loads will be supported by it, and $\Delta\phi_W$ is the difference of the perturbation potential of the upper and lower surfaces of the wake. By discretizing the body and wake surfaces into small elements and applying the collocation method, the perturbation potential at each aerodynamic collocation point (ACP) on the body may be expressed as

$$\phi_h = \sum_{k=1}^{n_B}\alpha_{hk}\phi_k + \sum_{k=1}^{n_W}\alpha_{h(k+n_B)}\Delta\phi_k + \sum_{k=1}^{n_B}\beta_{hk}\left(\frac{\partial\phi}{\partial\boldsymbol{n}}\right)_k \tag{5}$$

where coefficients α_{hk} and β_{hk} can be evaluated either analytically or numerically and the value of $\partial\phi/\partial\boldsymbol{n}$ is determined using the nonpenetration boundary condition at each body surface element.

Based on the Kelvin theorem, the value of $\Delta\phi_W$ for each wake element is the same value as its forward element at the last time step ($\Delta t = \delta/U_\infty$, where δ and U_∞ are the chordwise length of each wake element and the freestream velocity, respectively). Equation (5), in conjunction with the Kelvin theorem and Kutta condition, forms the governing equations of the aerodynamic system in the discrete-time domain, as follows:

$$\mathbf{A}\,\boldsymbol{\mu}^{n+1} + \mathbf{B}\boldsymbol{\mu}^{n} = \begin{bmatrix} \boldsymbol{w} \\ \mathbf{0} \end{bmatrix}^{n+1} \tag{6}$$

where $\mathbf{A}$ and $\mathbf{B}$ are the aerodynamic influence matrices, and $\boldsymbol{w}$ is the downwash vector at the body elements. Further, the vector $\boldsymbol{\mu}$ is defined as follows:

$$\boldsymbol{\mu} = [\phi_1, \phi_2, \ldots, \phi_{n_B}, \Delta\phi_1, \Delta\phi_2, \ldots, \Delta\phi_{n_W}]^T \tag{7}$$

A. Reduced-Order Modeling

Transforming the homogeneous part of Eq. (6) into the z domain and considering $\boldsymbol{\mu} = \boldsymbol{x}_i e^{\lambda_i t}$ and $z_i = e^{\lambda_i \Delta t}$, one can obtain the following eigenvalue problem:

$$\mathbf{AXZ} + \mathbf{BX} = \mathbf{0}, \qquad \mathbf{A}^T\mathbf{YZ} + \mathbf{B}^T\mathbf{Y} = \mathbf{0} \tag{8}$$

where $\mathbf{Z}$ is a diagonal matrix containing the eigenvalues and $\mathbf{X}$ and $\mathbf{Y}$ are the matrices containing the right and left eigenvectors, respectively. These eigenvectors are indeed the natural modes of the perturbation potential distribution over the aerodynamic computational domain. The modal formulation of the aerodynamic system must be modified with a static correction method to include at least the quasi-static contribution of the higher truncated modes [1], namely,

$$\boldsymbol{\mu} = \boldsymbol{\mu}_s + \boldsymbol{\mu}_d = \boldsymbol{\mu}_s + \mathbf{X}\boldsymbol{c} \tag{9}$$

where $\boldsymbol{c}$ is the vector of aerodynamic generalized coordinates. The quasi-static portion $\boldsymbol{\mu}_s$ is calculated as follows:

$$(\mathbf{A} + \mathbf{B})\boldsymbol{\mu}_s^n = \begin{bmatrix} \boldsymbol{w}^n \\ \mathbf{0} \end{bmatrix} \tag{10}$$

Substituting Eq. (9) into Eq. (6) and premultiplying by $\mathbf{Y}^T$ and using the orthogonality conditions, a set of uncoupled equations for the aerodynamic modal coordinates is obtained as follows:

$$\mathbf{c}^{\,n+1} - \mathbf{Z}\boldsymbol{c}^n = \mathbf{Y}^T\boldsymbol{w}^{n+1} - \mathbf{Y}^T\left(\mathbf{A}\boldsymbol{\mu}_s^{n+1} + \mathbf{B}\boldsymbol{\mu}_s^{n}\right) \tag{11}$$

Substitution of $\boldsymbol{\mu}_s$ from Eq. (10) into Eq. (11) gives

$$(\boldsymbol{c}^{n+1} - \boldsymbol{c}^n)(\mathbf{I} - \mathbf{Z})\boldsymbol{c}^n = \hat{\mathbf{Y}}\,\hat{\mathbf{B}}\,\hat{\mathbf{T}}(\boldsymbol{w}^{n+1} - \boldsymbol{w}^n) \tag{12}$$

where

$$\mathbf{Y}^T = [\ldots\ \hat{\mathbf{Y}}_{n_B \times n_W}], \quad \mathbf{B} = \begin{bmatrix} \mathbf{0} & \mathbf{0} \\ \mathbf{0} & \hat{\mathbf{B}}_{n_W \times n_W} \end{bmatrix}, \quad (\mathbf{A}+\mathbf{B})^{-1} = \begin{bmatrix} \mathbf{T}_{n_B \times n_B} & \cdots \\ \hat{\mathbf{T}}_{n_W \times n_B} & \cdots \end{bmatrix} \tag{13}$$

Dividing Eq. (12) by the time step and returning it into the continuous-time domain results in a system of equations that relates the aerodynamic modal coordinates to the downwash vector, as follows:

$$\dot{\boldsymbol{c}} + U_\infty\hat{\mathbf{K}}\boldsymbol{c} = \hat{\mathbf{Y}}\,\hat{\mathbf{B}}\,\hat{\mathbf{T}}\,\dot{\boldsymbol{w}} \tag{14}$$

where $\hat{\mathbf{K}}$ is a diagonal matrix given by

$$\hat{\mathbf{K}} = \delta^{-1}(\mathbf{I} - \mathbf{Z}) \tag{15}$$

B. Downwash

Considering a moving flexible body, the downwash at a point on the body surface can be written as follows:

$$w = -(U_\infty\boldsymbol{v} + \dot{\boldsymbol{e}}_r)\cdot\boldsymbol{n} \tag{16}$$

where $U_\infty\boldsymbol{v}$ indicates the velocity vector of the origin of the body-fixed frame, $\boldsymbol{e}_r$ is the elastic displacement vector, and $\boldsymbol{n}$ is the surface normal unit vector at this point. For infinitesimal elastic displacements, Eq. (16) can be rewritten as follows:

$$w = -U_\infty\boldsymbol{v}^T\boldsymbol{n}_0 - U_\infty\boldsymbol{v}^T\hat{\boldsymbol{n}} - \boldsymbol{n}_0^T\dot{\boldsymbol{e}}_r \tag{17}$$

where $\boldsymbol{n}_0$ is the undeformed surface unit normal vector and $\hat{\boldsymbol{n}}$ is the vector of the small variation of $\boldsymbol{n}_0$ that can be calculated as follows:

$$\hat{\boldsymbol{n}} = \boldsymbol{e}_\theta \times \boldsymbol{n}_0 = -\tilde{\boldsymbol{n}}_0\boldsymbol{e}_\theta \tag{18}$$

where $\boldsymbol{e}_\theta$ is the very small elastic rotation vector and the tilde indicates the cross-product operation in matrix form. Now Eq. (17) can be rewritten as follows:

$$w = -U_\infty\boldsymbol{v}^T\boldsymbol{n}_0 + U_\infty[\mathbf{0} \quad \boldsymbol{v}^T\tilde{\boldsymbol{n}}_0]\begin{bmatrix} \boldsymbol{e}_r \\ \boldsymbol{e}_\theta \end{bmatrix} - [\,\boldsymbol{n}_0^T \quad \mathbf{0}]\begin{bmatrix} \dot{\boldsymbol{e}}_r \\ \dot{\boldsymbol{e}}_\theta \end{bmatrix} \tag{19}$$

Applying the modal form of the structural displacements at the ith ACP yields

$$\begin{bmatrix} \boldsymbol{e}_r \\ \boldsymbol{e}_\theta \end{bmatrix}_i = \bar{\boldsymbol{\Psi}}_i\boldsymbol{q} \tag{20}$$

where $\bar{\boldsymbol{\Psi}}$ is the matrix of the structural mode shapes represented at the ACPs (including displacements and rotations) for which the columns contain the mode shapes, and $\bar{\boldsymbol{\Psi}}_i$ is the submatrix of $\bar{\boldsymbol{\Psi}}$ that is related to the ith ACP.

C. Interpolation

Recalling the fact that the aerodynamic and structural meshes do not usually coincide, an interpolation technique is required to transfer data between them. For this purpose, the transformation matrix $\mathbf{G}$ is used to convey the structural shape modes from the structural grid points (matrix $\boldsymbol{\Psi}$) to the ACPs, as follows:

$$\bar{\boldsymbol{\Psi}} = \mathbf{G}\boldsymbol{\Psi} \tag{21}$$

In this work, to determine the matrix $\mathbf{G}$, each ACP is connected to a proper structural element, and the element shape functions are used to obtain the displacements and rotations of the ACP in terms of those of the element nodes. This interpolation procedure is simple and effective in coupling the aerodynamic and structural grid points and avoids some of the problems associated with other methods (such as the splines technique) that are widely used [7]. The proposed method resolves the problem of using splines for complex curved surfaces such as aircraft wing-body interaction and excludes the errors of using spline derivatives. Overall, employing Eqs. (19–21), the vector of downwash on the ACPs can be written as follows:

$$\boldsymbol{w} = U_\infty\boldsymbol{w}_0 + U_\infty\mathbf{E}\boldsymbol{q} + \mathbf{F}\dot{\boldsymbol{q}} \tag{22}$$

D. Aerodynamic Loads

From Eqs. (9), (10), (13), and (22), one can state the vector of perturbation potentials as follows:

$$\bar{\boldsymbol{\mu}} = U_\infty\mathbf{T}\boldsymbol{w}_0 + U_\infty\mathbf{TE}\boldsymbol{q} + \bar{\mathbf{X}}\boldsymbol{c} + \mathbf{TF}\dot{\boldsymbol{q}} \tag{23}$$

where the overbar indicates the submatrix or vector related to the aerodynamic elements on the body. For small potential perturbations, the unsteady Bernoulli equation is simplified as follows:

$$\mathrm{C}_p = -\frac{1}{U_\infty^2}\left((\nabla\phi_\infty)^T\nabla\phi + 2\frac{\partial\phi}{\partial t}\right) \tag{24}$$

where $\nabla\phi_\infty$ is equal to the freestream velocity vector. The value of $\nabla\phi$ at each ACP can be calculated in terms of the perturbation potentials by using one of the finite difference schemes. Thus, the pressure coefficient on the ACPs is derived in the following vector form:

$$\boldsymbol{C}_p = -\frac{1}{U_\infty^2}(U_\infty \mathbf{O}\bar{\boldsymbol{\mu}} + \dot{\bar{\boldsymbol{\mu}}}) \tag{25}$$

where $\mathbf{O}$ is an operator matrix. The right-hand side of the structural system of equations is the vector of the generalized aerodynamic loads, which can be written by using the virtual work principle, as follows:

$$\boldsymbol{\Xi} = q_\infty \mathbf{S}\boldsymbol{C}_p \tag{26}$$

where $q_\infty = \rho U_\infty^2/2$ is the flow dynamic pressure, and $\mathbf{S}$ is an integration operator matrix. If the pressure coefficient is assumed to be constant within each aerodynamic element, the elements of the $\mathbf{S}$ matrix can be calculated as follows:

$$\mathbf{S}_{ij} = -s_j \boldsymbol{n}_{0_j}^T \boldsymbol{\Delta}_{ij} \tag{27}$$

where s_j is the area of the jth aerodynamic element, and $\boldsymbol{\Delta}_{ij}$ is the vector of displacement components of its collocation point at the ith structural mode shape. Finally, the combination of Eqs. (23), (25), and (26) yields the generalized loads for the structural system of equations, namely,

$$\boldsymbol{\Xi} = \rho\Big\{\mathbf{M}_a\ddot{\boldsymbol{q}} + (U_\infty \mathbf{C}_a\dot{\boldsymbol{q}} + \bar{\mathbf{C}}_a\dot{\boldsymbol{c}}) + \left(U_\infty^2 \mathbf{K}_a\boldsymbol{q} + U_\infty \bar{\mathbf{K}}_a\boldsymbol{c}\right) + U_\infty^2 \boldsymbol{f}\Big\} \tag{28}$$

where

$$\mathbf{M}_a = \mathbf{STF}, \qquad \mathbf{C}_a = \mathbf{S}\bar{\mathbf{X}}, \qquad \bar{\mathbf{C}}_a = \mathbf{SOTF} + \mathbf{STE}$$
$$\mathbf{K}_a = \mathbf{SO}\bar{\mathbf{X}}, \qquad \bar{\mathbf{K}}_a = \mathbf{SOTE}, \qquad \boldsymbol{f} = \mathbf{SOT}\boldsymbol{w}_0 \tag{29}$$

IV. Aeroelastic Modeling

Equations (1) and (28) form the structural part of the aeroelastic model, and substituting Eq. (22) into Eq. (14) gives the complementary aerodynamic equations set, as follows:

$$\hat{\mathbf{M}}\ddot{\boldsymbol{q}} + U_\infty \hat{\mathbf{C}}\dot{\boldsymbol{q}} + \dot{\boldsymbol{c}} + U_\infty \hat{\mathbf{K}}\boldsymbol{c} = \mathbf{0} \tag{30}$$

where

$$\hat{\mathbf{M}} = -\hat{\mathbf{Y}}\hat{\mathbf{B}}\hat{\mathbf{T}}\mathbf{F}, \qquad \hat{\mathbf{C}} = -\hat{\mathbf{Y}}\hat{\mathbf{B}}\hat{\mathbf{T}}\mathbf{E} \tag{31}$$

Defining the new state $\hat{\boldsymbol{q}}$ as $\hat{\boldsymbol{q}} = \dot{\boldsymbol{q}}$, the combination of Eqs. (1), (28), and (30) yields the reduced-order aeroelastic system of equations, as follows:

$$\mathbf{P}\dot{\bar{\boldsymbol{q}}} + \mathbf{R}\bar{\boldsymbol{q}} = \boldsymbol{Q} \tag{32}$$

where

Table 1 Dimensionless structural parameters of the wing

Parameter	Description	Value
σ	uncoupled bending-torsion frequency ratio	0.4
a	elastic axis location parameter	−0.2
x_α	dimensionless static unbalance	0.1
μ	density ratio	20
r_α	dimensionless radius of gyration of the wing section	0.5

$$\mathbf{P} = \begin{bmatrix} \mathbf{M}_s + \rho\mathbf{M}_a & \mathbf{C}_s + \rho U_\infty \mathbf{C}_a & \rho\bar{\mathbf{C}}_a \\ \hat{\mathbf{M}} & U_\infty\hat{\mathbf{C}} & \mathbf{I} \\ \mathbf{0} & \mathbf{I} & \mathbf{0} \end{bmatrix}, \qquad \bar{\boldsymbol{q}} = \begin{bmatrix} \hat{\boldsymbol{q}} \\ \boldsymbol{q} \\ \boldsymbol{c} \end{bmatrix}$$
$$\mathbf{R} = \begin{bmatrix} \mathbf{0} & \mathbf{K}_s + \rho U_\infty^2 \mathbf{K}_a & \rho U_\infty \bar{\mathbf{K}}_a \\ \mathbf{0} & \mathbf{0} & U_\infty\hat{\mathbf{K}} \\ -\mathbf{I} & \mathbf{0} & \mathbf{0} \end{bmatrix}, \qquad \boldsymbol{Q} = \begin{bmatrix} \rho U_\infty^2 \boldsymbol{f} \\ \mathbf{0} \\ \mathbf{0} \end{bmatrix} \tag{33}$$

The resultant aeroelastic model can be used to determine the instability boundary and the aeroelastic time response. In addition, the state-space form of Eq. (32) makes it very useful for aeroservoelastic purposes.

V. Numerical Results

To examine the validity and capability of the proposed approach, three cases are investigated and the instability conditions are determined. For all examples, the NACA 0012 wing section is used and the wing structure is modeled as a uniform beam, with the dimensionless parameters given in Table 1. The wake length is equal to 10 times the chord length and is discretized by 40 elements in the streamwise direction. The desirable convergence criteria are satisfied using 4 structural mode shapes and 20 aerodynamic eigenmodes in these test cases.

These configurations are selected for flutter boundary determination using the present ROM in comparison with the NASTRAN doublet lattice method (DLM) for similar structural elements and aerodynamic grid arrangement. NASTRAN uses slender body theory to evaluate the body effect on the wing unsteady pressure distribution, because the DLM cannot be used for body aerodynamic modeling. The P-K flutter analysis method of NASTRAN is used to calculate approximate true aeroelastic damping in comparison with the P-method results of the present ROM.

A. High-Aspect-Ratio Wing-Body Configuration

Figure 1a shows a wing-body configuration aerodynamic mesh with a high-aspect-ratio wing. The body diameter ratio (ratio of the body diameter to the wing chord) is 0.4 and the wing aspect ratio is 7. The wing is discretized by 16 elements chordwise and 50 elements spanwise. The body is assumed to be a fixed rigid surface, and the

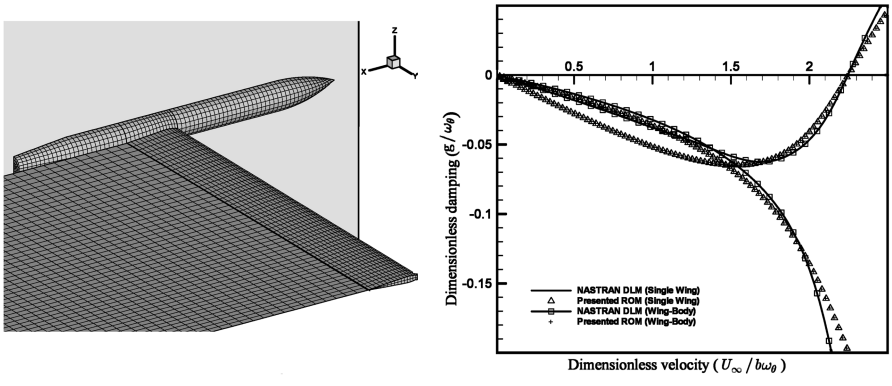

a) b)

Fig. 1 Geometry and U-g graphs of the high-aspect-ratio wing-body combination.

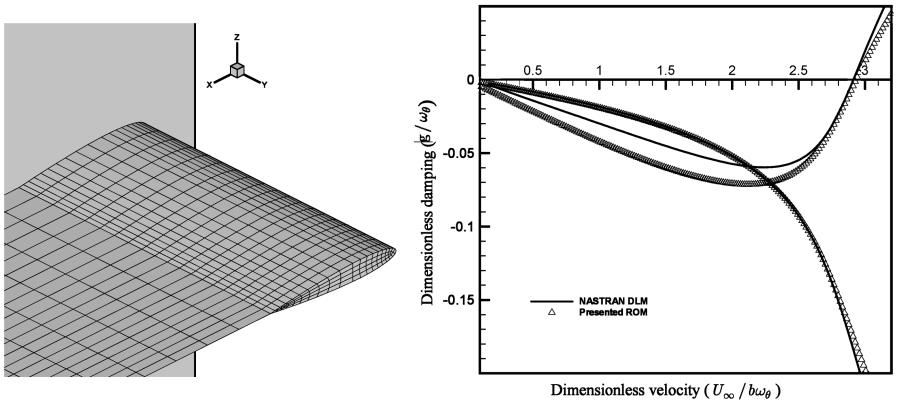

a) b)

Fig. 2 Geometry and U-g graphs of the low-aspect-ratio wing.

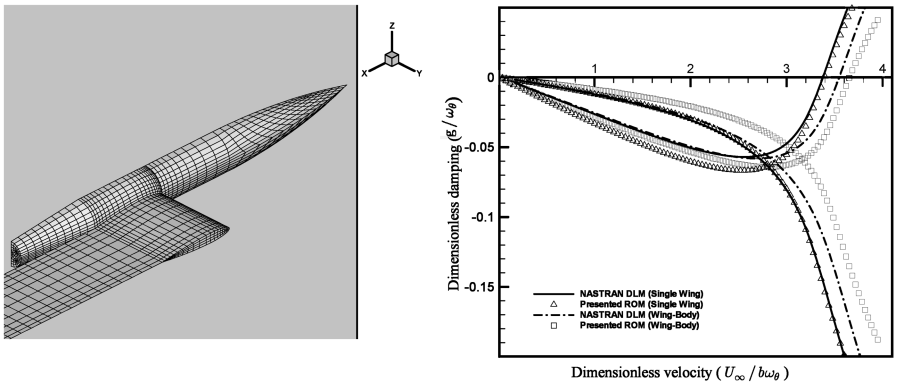

a) b)

Fig. 3 Geometry and U-g graphs of the low-aspect-ratio wing-body combination.

wing structure is simulated as a beam clamped to the fuselage side. The damping and freestream velocity values have been non-dimensionalized by the first torsional frequency of the structure (ω_θ, and $b\omega_\theta$, respectively, where b is the semichord of the wing). Figure 1b illustrates the U-g graphs obtained from the present ROM and NASTRAN for both the wing-body combination and the single wing with the same exposed aspect ratio. The dimensionless flutter speed of the wing-body configuration and the single wing is 2.23 using both methods, which indicates that the two methods yield the same results for high-aspect-ratio wings. The difference between the damping in each branch is due to the nature of P and P-K methods.

B. Low-Aspect-Ratio Wing

In this section, a low-aspect-ratio wing is examined for determination of aeroelastic instability. The wing aspect ratio is 2 and its upper and lower surfaces are discretized by 400 boundary elements, as shown in Fig. 2a. The similar flat geometry and aerodynamic grid is used to compare the NASTRAN result with that of our ROM, and the wing structure is modeled as a cantilever beam in a manner similar to the previous example. The U-g graphs obtained from both stability analysis methods are given in Fig. 2b, which indicates a dimensionless flutter speed of 2.91 using NASTRAN and 2.93 using our ROM. This example shows that in the absence of body, both methods also yield the same flutter speed for the low-aspect-ratio wings.

C. Low-Aspect-Ratio Wing-Body Configuration

The last test case is used to evaluate the validity of the introduced ROM results in the case of low-aspect-ratio wing-body configuration. The body diameter ratio is 0.4 and the wing aspect ratio is 1. The aerodynamic boundary element grid of this configuration is shown in Fig. 3a. The wing structure is modeled similar to the aforementioned examples, and the wing is clamped to the side of the fuselage, which is assumed to be rigid. The wing-body U-g graphs are plotted in comparison with those of a similar single wing with the same exposed aspect ratio and structure in Fig. 3b. The U-g graphs show that both methods yield the dimensionless flutter speed of about 3.38 for the wing alone. For the wing-body model, NASTRAN shows an increase of 5.7% above the flutter speed of the wing alone, whereas the present ROM shows an 8.1% flutter-speed increment. This difference may be the result of the difference between the slender body theory and the boundary element method used for body aerodynamic simulation in this paper.

An investigation of the considered examples illustrates an increase of the flutter speed with a decrease of the wing aspect ratio, as is expected. It can also be observed from the instability analysis results that the low-aspect-ratio wing-body configuration has a slightly higher flutter speed than the wing alone, and this difference vanishes as the aspect ratio increases.

Overall, there exists a good agreement between the results of the introduced ROM and NASTRAN for flutter determination, which validates our ROM. However, the subcritical damping of the present model is more accurate because of improved aerodynamic modeling and because of the state-space-form representation of the aeroelastic equations, which allows using the P method instead of the P-K method.

VI. Conclusions

In this research, a reduced-order aeroelastic model was developed using FEM-based modal analysis of structural dynamics and BEM-based fluid eigenanalysis method. This model is represented in a continuous-time domain state-space form, which is of more practical use for modeling of aeroelastic and aeroservoelastic systems, due to the more accurate evaluation of subcritical damping. In this regard, the introduced ROM needs no static corrections in each time step. The used BEM aerodynamic modeling approach is capable of

simulating arbitrary streamlined body aerodynamics, in comparison with the limited application of the slender body theory, which is widely used in the incompressible flow regime. The employed interpolation technique is simple and effective to couple the structural and aerodynamics grids for complex geometries. Because of the advantages of the reduced-order modeling techniques, the introduced ROM can also be used in iterative processes such as structural layout design and aeroelastic optimization. Three configurations are examined for flutter calculation using the presented ROM, and comparison with NASTRAN results shows a good agreement. The results confirm that a decrease of wing aspect ratio leads to an increase of the flutter speed. Also, the numerical results obtained from the employed modeling approach show that for low-aspect-ratio cases, the flutter speed of the wing in the presence of a body is slightly higher than the wing alone when equal structures and exposed aspect ratios are considered.

Acknowledgment

The authors acknowledge Sharif University of Technology for financial support of this research (grant 7100/2066).

References

[1] Hall, K. C., "Eigenanalysis of Unsteady Flows about Airfoils, Cascades, and Wings," *AIAA Journal*, Vol. 32, No. 12, 1994, pp. 2426–2432.

[2] Romanowski, M. C., and Dowell, E. H., "Reduced Order Euler Equations for Unsteady Aerodynamic Flows: Numerical Techniques," Aerospace Sciences Meeting and Exhibit, 34th, Reno, NV, AIAA Number 96-0528, Jan. 1996.

[3] Romanowski, M. C., "Using Fluid Eigenmodes to Develop Euler Based Reduced Order Unsteady Aerodynamic and Aeroelastic Models," Ph. D. Dissertation, Duke Univ., Durham, NC, 1995.

[4] Hall, K. C., and Romanowski, M. C., "Eigenmode Analysis in Unsteady Aerodynamics: Reduced Order Models," *Applied Mechanics Reviews*, Vol. 50, No. 6, 1997, pp. 371–385.

[5] Heeg, J., and Dowell, E. H., "Aerodynamic and Aeroelastic Insights Using Eigenanalysis," 40th AIAA/ASME/ASCE/AHS/ASC Structures, Structural Dynamics, and Materials Conference, St. Louis, MO, AIAA Paper 99-1473, Apr. 1999.

[6] Esfahanian, V., and Behbahani-nejad, M., "Reduced Order Modeling of Unsteady Flows About Complex Configurations Using the Boundary Element Method," *Journal of Fluids Engineering*, Vol. 124, No. 4, 2002, pp. 988–993.

[7] Rodden, W. P., and Johnson, E. H., *MSC/NASTRAN Aeroelastic Analysis User's Guide, Ver. 68*, The MacNeal/Schwendler Corp., Los Angeles, 1994.